HHS Public Access

Author manuscript

Transl Stroke Res. Author manuscript; available in PMC 2024 October 01.

Published in final edited form as:

Transl Stroke Res. 2023 October ; 14(5): 704–722. doi:10.1007/s12975-022-01092-7.

Deferoxamine Prevents Neonatal Posthemorrhagic Hydrocephalus Through Choroid Plexus-Mediated Iron Clearance

Sruthi Ramagiri, PhD[1,*], **Shelei Pan**[1,*], **Dakota DeFreitas, MA**[1,*], **Peter H. Yang, MD**[1], **Dhvanii Raval**[1], **David Wozniak, PhD**[2,3,4], **Prabagaran Esakky, PhD**[1], **Jennifer M Strahle, MD**[1,5,6]

[1]Department of Neurosurgery, Washington University School of Medicine, Washington University in St. Louis, St. Louis, MO 63110, USA

[2]Department of Psychiatry, Washington University School of Medicine, St. Louis, MO 63110-1093, USA

[3]Intellectual and Developmental Disabilities Research Center, Washington University School of Medicine, St. Louis, MO 63110-1093, USA

[4]Taylor Family Institute for Innovative Psychiatric Research, Washington University School of Medicine, St. Louis, MO 63110-1093, USA

[5]Department of Orthopedic Surgery, Washington University School of Medicine, Washington University in St. Louis, St. Louis, MO 63110, USA

[6]Department of Pediatrics, Washington University School of Medicine, Washington University in St. Louis, St. Louis, MO 63110, USA

Abstract

Posthemorrhagic hydrocephalus occurs in up to 30% of infants with high-grade intraventricular hemorrhage and is associated with the worst neurocognitive outcomes in preterm infants. The mechanisms of posthemorrhagic hydrocephalus after intraventricular hemorrhage are unknown; however, CSF levels of iron metabolic pathway proteins including hemoglobin have been implicated in its pathogenesis. Here, we develop an animal model of intraventricular hemorrhage using intra-ventricular injection of hemoglobin at post-natal day 4 that results in acute and chronic hydrocephalus, pathologic choroid plexus iron accumulation, and subsequent choroid plexus injury at post-natal days 5, 7, and 15. This model also results in increased expression of aquaporin-1, Na+/K+/Cl- cotransporter 1, and Na+/K+/ATPase on the apical surface of the choroid plexus 24 h post-intraventricular hemorrhage. We use this model to evaluate a clinically relevant treatment strategy for the prevention of neurological sequelae after intraventricular hemorrhage using intraventricular administration of the iron chelator deferoxamine at the time of hemorrhage. Deferoxamine treatment prevented posthemorrhagic hydrocephalus for up to 11 days after intraventricular hemorrhage and prevented the development of sensorimotor gating

Corresponding Author: Jennifer M. Strahle, Strahlej@wustl.edu.
*These authors contributed equally: Sruthi Ramagiri, Shelei Pan, Dakota DeFreitas

Competing interests
The authors report no competing interests.

deficits. In addition, deferoxamine treatment facilitated acute iron clearance through the choroid plexus and subsequently reduced choroid plexus iron levels at 24 h with reversal of hemoglobin-induced aquaporin-1 upregulation on the apical surface of the choroid plexus. Intraventricular administration of deferoxamine at the time of intraventricular hemorrhage may be a clinically relevant treatment strategy for preventing posthemorrhagic hydrocephalus and likely acts through promoting iron clearance through the choroid plexus to prevent hemoglobin-induced injury.

Keywords

Hydrocephalus; germinal matrix hemorrhage; preterm; intraventricular hemorrhage; deferoxamine

1. Introduction

Neonatal germinal matrix hemorrhage-intraventricular hemorrhage (GMH-IVH) is a significant cause of morbidity and mortality and is associated with the worst neurodevelopmental outcomes of those born preterm [1, 2]. Neurologic sequelae of GMH-IVH include cognitive deficits, cerebral palsy, and posthemorrhagic hydrocephalus (PHH), the latter of which develops in up to 30% of children with high-grade GMH-IVH [3]. We have previously shown hemoglobin (HB) and iron-mediated development of PHH after IVH in animal models and have recently validated these preclinical findings in two separate patient cohorts, implicating iron metabolism as a key pathway in altering CSF circulation resulting in PHH [4–9]. However, the long-term consequences of IVH in the preclinical setting are not known nor are the specific mechanisms by which iron is cleared. Current treatment of PHH is palliative (surgery for CSF diversion), often associated with complications, and does not prevent initial brain injury from IVH [3, 10–13]. As the timing of IVH and subsequent development of PHH in preterm infants is well-known and anticipated, there is an opportunity for treatment at the time of injury [14, 17–19, 21, 25].

A major challenge in developing effective treatment strategies in the preclinical setting is the selection of an appropriate drug and administration method with known in vivo performance and clearance mechanisms [14, 19, 26]. Deferoxamine (DFX), an injectable iron chelator, is used to treat patients with iron-overload syndromes such as hemochromatosis and thus is already in clinical use [22]. DFX plays a physiologic role similar to that of ferritin and sequesters free iron thereby reducing iron-mediated production of free radicals and down-stream DNA damage, cell death, and neurotoxicity [16, 20, 22, 23, 25]. Free-radical scavengers can help protect against iron-mediated hydrocephalus and behavioral deficits [27], and DFX may also act through this mechanism to prevent free-radical damage to the ventricular system through iron chelation [28]. Importantly, intraventricular DFX clearance has been shown to occur via native drug transport mechanisms of the choroid plexus (ChP) epithelium, making this an attractive pathway that could be harnessed for therapeutic purposes, particularly in light of recent evidence supporting ChP-mediated CSF solute clearance during development [24, 29].We previously showed improvement in ventricle size in a neonatal (P7) IVH model with early peripheral DFX treatment, and others have reported similar outcomes [8, 17]. However, while intraventricular DFX treatment has been reported in one adult IVH [27] and one adult subarachnoid hemorrhage preclinical study [18], it

has not been evaluated during development in neonatal GMH-IVH-PHH, nor has it been evaluated at the time of IVH [21]. Direct application of DFX into the ventricle may be a viable targeted strategy to prevent ventricular dilation and brain injury by utilizing the inherent clearance mechanism of the ChP and the physical proximity of an iron chelation agent to the heme–iron burden in the brain ventricles.

In this study, we show that intraventricular HB administration results in progressive and chronic ventricular enlargement in a neonatal rat model of GMH-IVH in a clinically mimetic manner to PHH. We furthermore show that intraventricular DFX treatment at the time of injury facilitates early clearance of iron through the ChP, maintains normal CSF solute clearance through the ChP, delays hydrocephalus for 11 days after injury, and prevents long-term sensory-motor gating deficits. Ventricular DFX administration represents a clinically feasible treatment strategy and likely acts through promotion of iron clearance from the ventricles via the ChP.

2. Results

2.1 HB alters CSF distribution within the ventricular system and results in acute and chronic hydrocephalus

Intraventricular injection of 20 μL HB (150 mg/mL) in P4 rats resulted in lateral ventricle (LV), third ventricle (3V), and cavum septum pellucidum (CSP) dilation compared to artificial CSF (aCSF)-injected animals at 72 h post-injection (Figs. 1B, C and 2C, D, G). The significant increase in LV volume was sustained up to P21 (Fig. 3B, D); however, by P60, there was a wide range in LV volumes representative of two cohorts: one in which ventriculomegaly resolved and another in which there was sustained ventriculomegaly (Fig. 3F). However, the rate of hydrocephalus in HB-injected rats, defined as 3 standard deviations above the mean of aCSF-injected rats [30], was significantly increased compared to the rate of hydrocephalus in aCSF-injected rats at both P21 and P60 ($p = 0.0079$, Fisher's exact test) (Fig. 3E, G). Importantly, this wide distribution of ventricle sizes indicates long-term variation in response to IVH, which recapitulates clinical rates of PHH development following IVH in preterm infants [3].

Furthermore, as HB was injected unilaterally into the right LV, we compared right and left LV volumes 72 h (P7), 11 days (P15), and 17 days (P21) after HB injection and found bilateral ventriculomegaly with no volumetric differences between the two sides (Supplementary Fig. 1). The cerebral aqueduct was visualized in all animals on T2-weighted MRI (Fig. 2A), and there was no difference in 4V volume following HB injection (Fig. 2H). Notably, cortical volumes were similar in all groups 72 h after injection (Fig. 2E). The specific ventricular expansion response between ventricles (LVvs. 3V vs. 4V) may indicate inherent differences in regional ependymal tissue response to HB.

2.2 Intraventricular DFX at time of IVH prevents early hydrocephalus

As neonatal preterm IVH occurs during a specific time window after birth, we evaluated treatment with intraventricular iron chelation with DFX at the time of IVH induction (Fig. 1A). To determine the effect and dose response of intraventricular DFX on the development

of PHH following IVH, we evaluated six different doses of DFX ranging from 0.4 to 20.0 mg/kg (Fig. 1B). All doses were injected into the right LV at the time of IVH (Fig. 1B and C). DFX doses ranging from 0.4 to 5.0 mg/kg were effective at preventing PHH 72 h post-injection (Fig. 1C). CSF accumulation in the CSP specifically was also prevented by DFX treatment (Fig. 2D). Higher concentrations of DFX (10.0 mg/kg and 20.0 mg/kg) did not prevent ventricular enlargement and resulted in ventricular enlargement com-parable to that of the HB group, likely due to toxicity (Fig. 1C). One milligram per kilogram of DFX was the lowest dose effective at preventing ventricular enlargement and was used for all subsequent experiments. No mortality or toxicity was observed with 1.0 mg/kg DFX; all animals were healthy and active, and no changes in the ventricular system were observed when 1.0 mg/kg DFX was injected alone (Fig. 1B, C).

Treatment with 1.0 mg/kg DFX at the time of IVH induction (HB+DFX) resulted in a significant decrease in ventricle size 72 h post-injection compared to animals injected with HB only (Fig. 2C). Consequently, the rate of hydrocephalus in DFX-treated animals (0 of 9 animals) was significantly decreased compared to HB-injected animals (6 of 9 animals) (Supplementary Fig. 2, Supplementary Table 1). This effect was sustained up to 11 days post-IVH (P15), where none of the animals treated with DFX developed hydrocephalus (0 of 8 animals) while 10 of 18 animals that were not treated with concurrent DFX developed hydrocephalus ($p = 0.0095$, Fisher's exact test) (Fig. 2I, J, Supplementary Table 2).

Treatment with DFX did not prevent the eventual onset of progressive ventricular enlargement at P21 and P60 (Fig. 3A, D, F). However, at these later time points, there was a wide distribution of ventricular volumes in the HB + DFX group, indicating possible efficacy of DFX in preventing chronic ventricular dilation in a subset of rats.

2.3 DFX does not prevent ChP injury after intraventricular HB injection.

Because the ChP is believed to have a role in CSF clearance during post-natal development in addition to its canonical role in CSF production, we examined the effect of aCSF, HB, HB + DFX, and DFX injection on the LV ChP. At 24 h, 72 h, and 11 days after HB injection, the ChP luminal diameter was decreased compared to that of aCSF animals (Fig. 4A, C, D, E). There was also increased disruption of the ChP structure 72 h post-HB injection (22.1 ± 5.3% of the ChP structure) compared to aCSF controls (5.2 ± 1.9%) (Fig.4F, G). No changes in ChP structure were observed 6 h post-HB injection (Fig.4B).

Despite its therapeutic effect against PHH development, DFX treatment did not prevent the HB-induced decrease in ChP luminal diameter, nor did it prevent HB-induced ChP structural injury at 24 h, 72 h, and 11 days post-HB injection (Fig. 4A–G). Qualitatively, the ChP in the HB and HB + DFX groups had less interaction with the LV wall compared to aCSF-injected animals at all timepoints. DFX injection alone did not result in quantifiable changes to the ChP compared to aCSF-injected animals (Fig. 4). Finally, in contrast to the HB-induced ChP structural changes, there was no significant structural injury to the LV ependymal surface (Fig. 4H, I).

2.4 DFX mediates early iron clearance through the ChP in IVH

We evaluated the ChP as a potential iron clearance route, as intraventricular DFX has been previously shown to be cleared through the ChP [28]. Little to no ferric iron was observed in the ChP of rats injected with only aCSF or DFX at any time point (Fig. 5), indicating that baseline iron levels within the ChP are low and that DFX alone does not impact physiologic iron clearance. After HB injection, however, there was a significant increase in epithelial ChP iron at all time points after 6 h compared to aCSF controls (Fig. 5C–E).

In HB + DFX-injected rats, there was a significant increase in iron in the ChP lumen 6h post-injection compared to aCSF-injected rats (Fig. 5B). There was also increased luminal ChP iron in HB+DFX rats compared to HB-injected rats, in which iron was primarily located within the ChP epithelial cells (Fig. 5A). Twenty four hours after injection, there was significantly less ChP iron in HB + DFX-injected rats compared to HB-injected rats (Fig. 5C). After this time point, there was a sustained decrease in ChP iron in the HB + DFX group compared to the HB group until P15 (Fig. 5D, E). Significant iron deposition in the periventricular ependyma, hippocampus, or cortex was not observed at any of the experimental time points with Perl's staining.

To assess possible neuroinflammatory changes in the ChP secondary to increased ChP iron after HB + DFX treatment, we examined the levels of inflammatory cytokine interleukin-6 (IL-6) at 2 h and 6 h post-HB injection. There was a significant elevation of ChP IL-6 at both timepoints in HB-injected animals compared to aCSF-injected animals (Fig. 5F, G). Treatment with DFX at the time of HB injection trended towards lowered IL-6 expression at 2 h post-injection (Fig. 5F) and did not result in significantly increased IL-6 expression over HB-injection levels at 6 h post-injection (Fig. 5G), suggesting that the increased ChP luminal iron at 6 h did not result in unintended inflammatory changes.

Taken together with our findings of retained ChP structural integrity at 6 h post-HB injection, the ChP may not only retain the ability to clear HB (and thereby iron) early after IVH, but also provides a route by which expedited clearance can occur, as seen by the elevated iron content primarily within the ChP lumen at this time point. Further-more, this enhanced ability to clear iron in the presence of DFX early after IVH is followed by a reduction in ChP iron at all later time points, which suggests diminished egress as a result of a lower iron burden within the ventricles.

2.5 DFX reverses reduced CSF solute clearance through the ChP after IVH.

1.9-nm gold nanoparticles (AuNPs) (Nanoprobes, Yaphank, NY) were injected into the right LV at P7 (72 h after CSF, HB, and HB + DFX injections) in order to track CSF solute clearance in a subset of rats. AuNPs were primarily observed in the ChP lumen in aCSF animals, suggesting this location as the site of CSF solute trafficking and subsequent clearance by the ChP. In HB-injected animals, we observed a significant increase in AuNPs retained in the ChP epithelial cells compared to aCSF control animals, indicating impaired CSF solute clearance through the ChP after IVH (Fig. 6). Treatment with DFX was associated with reduced ChP AuNPs compared to HB rats (Fig. 6C), indicating preserved ChP CSF solute handling and clearance several days after DFX administration.

2.6 ChP apical expression of ion and water transporters precede significant ventricular expansion after IVH

To assess the functional capacity of the ChP after IVH, we evaluated the apical surface of the ChP using immunofluo-rescence. We found a significant increase in the expression of aquaporin-1 (AQP1), Na+/K+/ATPase (NKAT), and Na+/K+/Cl- cotransporter 1 (NKCC1) along the apical surface of the ChP in HB-injected animals 24 h post-injection (Fig. 7A, B). No differences were observed at 72 h (Fig. 7C). Treatment with DFX at the time of HB injection was associated with a reduction in HB-induced AQP1 expression at 24 h but did not alter NKAT or NKCC1 expression (Fig. 7B).

Quantitative analysis of protein expression in intact and non-intact ChP showed that AQP1 and NKAT expression were decreased 24 h post-HB injection compared to aCSF controls (Supplementary Fig. 3A, B). No significant differences in NKCC1 expression were observed at 24 h (Supplementary Fig. 3C). NKAT and NKCC1 expression were decreased 72 h post-HB injection (Supplementary Figure 3F, G); however, no significant differences in AQP1 expression were observed (Supplementary Fig. 3E). No significant differences in protein expression of AQP1, NKAT, and NKCC1 were observed between HB and HB + DFX animals 24 and 72 h post-injection (Supplementary Fig. 3).

The finding of an overall decrease in protein levels of AQP1, NKAT, and NKCC1 within the entire ChP likely reflects the overall state of ChP damage after HB injection (IVH) compared to our functional quantification of the intact ChP apical surface. Furthermore, there was a significant increase in the number of apoptotic LV ChP cells at 24 h and 72 h after HB injection (Fig. 7D–F). DFX treatment did not reduce the number of apoptotic cells at either timepoint (Fig. 7E, F).

2.7 Neonatal IVH-PHH produces iron-mediated behavioral effects in HB-injected rats

Similar to clinical preterm IVH, intraventricular HB injection did not result in significant sensorimotor deficits (walking initiation, ledge, large platform, small platform, or inverted screen tests) in adolescent rats compared to the aCSF control group (Supplementary Fig. 4A, B, C, D). However, with DFX treatment, HB + DFX rats spent significantly less time on the 90° inclined screen compared to either the HB ($p = 0.010$) or aCSF ($p = 0.002$) groups (Supplementary Fig. 4E), suggesting deficits in strength and/or coordination in the HB + DFX rats. Importantly, this possible sensorimotor deficit in the HB + DFX rats did not impair their performance on aspects of more cognitively based tests (e.g., cued performance, swimming speeds in the Morris water maze (MWM)) or with regard to the acoustic startle or pre-pulse inhibition (PPI) responses (Supplementary Fig. 4H, I; Fig. 8). There were no consistent differences between groups concerning spatial learning acquisition (place trials-MWM) or anxiety-like behaviors (elevated plus maze (EPM) testing) (Supplementary Fig. 4F, G (EPM), J (MWM)). While DFX treatment did not have demonstrable effects on spatial learning and memory performance in HB-injected rats, treatment at time of IVH with DFX improved HB-induced diminished acoustic startle and PPI responses. Specifically, impaired acoustic startle responses in HB-injected rats were increased to aCSF control-like levels with DFX treatment (HB vs. HB + DFX ($p = 0.015$), and aCSF vs. HB ($p = 0.023$) groups), with similar magnitudes being exhibited by HB + DFX-treated and aCSF control

rats, suggesting a protective effect of DFX on impaired startle reactivity of HB rats (Fig. 8A). Similarly, total mean %PPI responses of the HB + DFX rats were significantly elevated relative to the HB group for the 8 dB ($p = 0.008$) and 16 dB ($p = 0.018$) above background PPI trials, and were similar to aCSF control levels (Fig. 8B).

Comparable results were found using a different method to calculate %PPI (Fig. 8C). In summary, treatment with DFX at time of IVH reversed behavioral deficits in HB-injected rats, specifically for acoustic startle and PPI responses.

3. Discussion

In this study, intraventricular DFX at the time of IVH injury in neonatal rats prevented early hydrocephalus, facilitated iron and CSF solute clearance through the ChP, and reduced neurologic dysfunction at 60 days. While DFX treatment did not alter HB-mediated ChP structural injury, it prevented IVH-induced ChP AQP1 increased expression. In summary, DFX maintained and facilitated ChP function early after injury, with important implications for clinical treatment strategies for the prevention of IVH-induced brain injury and hydrocephalus, and for understanding the role of ChP during development in clearance of CSF and drug-mediated intraventricular blood products.

In a neonatal rat model of GMH-IVH, intraventricular DFX treatment at the time of IVH prevented both hydrocephalus development for up to 11 days and impairment in long-term sensorimotor reactivity and gating, likely via expedited iron clearance by the ChP. Our model and experimental administration of intraventricular DFX uniquely address prevention of IVH-induced brain injury and PHH [8, 19, 31, 32]. Unlike older animals used in other studies, rat pups used in our study underwent intraventricular administration of HB at P4, which corresponds to the late second trimester/early third trimester in humans, a critically important developmental period in which infants born prematurely are at risk for GMH-IVH [19, 33]. As early CSF HB levels in preterm infants with IVH are associated with later development of PHH, we chose HB to model IVH [7]. Our final imaging endpoint of P60, corresponding to late adolescence in humans, allows for both tracking of ventricle size using serial in vivo MRIs and for the assessment of long-term neurological changes.

DFX administration directly into the ventricle bypasses the blood–brain-barrier, is in close proximity to the drug target (IVH) and allows for lower drug concentrations [18]. As (1) preterm IVH occurs during a defined time period (1–3 days after birth) and then progresses in the subsequent days and (2) HB causes significant bilateral ventricular enlargement within 24 h post-injection [8], we chose to co-inject DFX with HB to evaluate initiation of treatment at the earliest possible time point. We selected the lowest consistently effective DFX dose (1.0 mg/kg) to avoid toxicity after determining that doses of 1.0 mg/kg, 3.0 mg/kg, and 5.0 mg/kg were equivalent in preventing hydrocephalus [18]. Our HB IVH model resulted in chronic PHH similar to what is observed in humans and allowed us to examine specific biological changes in GMH-IVH without and with iron chelation.

The development of PHH following GMH-IVH is likely governed by multiple interrelated processes including astrogliosis, water/ion channel dysfunction, excess free-radical

production, and glymphatic impairment. Mitigating contributors to these processes, such as free-radical scavenging, have been shown to alleviate ventricular expansion [4, 8, 27, 32, 34–37]. However, iron-mediated ChP injury may be a common denominator initiating this complex cascade of events, and no studies to date have specifically investigated intrinsic solute clearance mechanisms during development for their disease-modifying potential. ChP function has traditionally been viewed as a source of CSF production [38]. In fact, the ChP has been shown to clear various solutes and drugs such as iron, antibiotics, amyloid-beta, and DFX and more recently CSF during development through NKCC1 [15, 24, 28, 29, 38–40]. Finally, the role of ChP in neurodegenerative disease has only recently begun to be elucidated: reduced ChP volume has been correlated with increased CSF levels of proteins important in pathophysiology of Alzheimer's and Parkinson's diseases, and impaired clearance of CSF tracer via the ChP has been found in patients with normal pressure hydrocephalus, and further implicates the ChP in solute clearance [42, 43].

We show iron and tracer clearance through the ChP, which is concurrent to ChP injury in our IVH model. Intra-ventricular HB without DFX resulted in continued iron accumulation in the ChP, peaking 72 h after injection. Specifically, iron was found almost exclusively outside the lumen within the epithelial cells of ChP at all-time points, indicating impairment in iron transport and prolonged contact between epithelial cells and free iron. The presence of intra-ventricular HB in all rats (without and with DFX) resulted in ChP damage in a time-dependent manner starting at 24 h, which likely contributed to ChP clearance dysfunction and downstream effects on CSF circulation resulting in hydro-cephalus. Intraventricular injection of AuNPs 72 h after induction of IVH resulted in an increase in tracer within the ChP 10 min after AuNP administration, suggesting ChP-mediated solute handling with impaired solute/CSF clearance in our IVH condition. This diminished ability of the ChP to clear solutes was associated with enlarged ventricles on MRI at this time point. An alternative explanation for our findings is the enhanced clearance of solutes after IVH; however, this is less likely as we found significant ventricular expansion at this time point.

Clinically relevant doses of intraventricular DFX at the time of HB administration (IVH) resulted in significantly more iron in the ChP 6 h after injection when compared to controls. Interestingly, iron was observed primarily inside the ChP lumen outside the epithelial cells, likely indicating trans-ChP transport of DFX-iron complexes into the lumen through known DFX transport mechanisms in the ChP [17, 21, 24, 28]. Although Perls staining does not distinguish between free iron and iron sequestered by DFX, these pat-terns suggest that prior to 24 h after injury, HB-derived free iron was sequestered by DFX and transported across the ChP epithelium into the lumen. This peak in iron clearance was followed by a decrease in iron levels within the ChP when compared to the HB group at 24 h and 72 h post-injury indicating expedited clearance of iron from the ventricle with DFX treatment. DFX also preserved some degree of functional integrity of the ChP at 72 h post-injury, whereby ChP AuNP levels were similar to that of the CSF control group, likely indicating CSF solute clearance similar to CSF-injected rats. Our interpretation of this finding is in the context of small ventricle sizes of DFX-treated HB rats and the CSF group in earlier time points, which suggests that the ChP retains its ability to clear solutes and contributes to the regulation of ventricular volume. These results, combined with our recent clinical study which showed that preserved ChP function through the production of CSF transferrin was associated with

improved neurocognitive outcomes in infants with PHH, may have implications for ChP cauterization for the treatment of neonatal hydrocephalus [9].

Despite the retained ability of the ChP to clear DFX-iron in the acute setting and prevent early hydrocephalus, the ChP continued to exhibit significant damage over time (unlike the ependyma which was not significantly injured), and ventricular enlargement at P21 and P60 was not able to be prevented by a single DFX dose at P4. In fact, ventricle volumes in the HB + DFX co-injected group, while small and equivalent to that of aCSF-injected rats at P7, increased by P21 and were equivalent to the degree of ventriculomegaly seen in HB-injected rats at P60. ChP expression of NKAT and NKCC1 was acutely increased at 24 h in the presence of intraventricular HB, but all trans-porter levels were equivalent to those in aCSF-injected rats at 72 h. ChP CSF production is driven by osmotic gradients produced primarily by carbonic anhydrase and NKAT [44, 46]. NKCC1 is a bidirectional ion transporter, and phosphorylated NKCC1 has recently been shown to mediate CSF clearance during postnatal development [29, 45]. In our model, the acute upregulation of NKCC1 in both the HB and HB + DFX groups suggests iron independent regulation of ion transporters involved with ChP CSF production and clearance. This response may be a maladaptive response of hypersecretion or an attempt at facilitating clearance of CSF. The latter interpretation is favored in the setting of DFX treatment as we show functional improvement in ChP solute clearance. Targeting ChP ion transport proteins that are upregulated in hydrocephalus has been shown to alleviate hydrocephalus in a kaolin animal model and is an area of active research [29]. However, more studies are needed on the directionality of CSF movement at the level of the ChP in hydrocephalus [29].

AQP1 is a selective water channel protein in the ChP and is upregulated in certain types of hydrocephalus in humans [36, 47]. We show that HB-induced AQP1 upregulation in the ChP 24h after IVH was prevented by intraventricular DFX treatment at time of IVH. AQP1 upregulation in the hours after IVH may indicate a hypersecretion phenomenon, and DFX may act as a regulatory agent in controlling maladaptive CSF hypersecretion through clearance of iron. ChP epithelial cells contain iron-responsive element-binding proteins that have reduced binding affinity in the presence of high iron loads in the CSF and may relate to overall dysregulation in ChP iron handling [38, 48, 49]. The sodium-coupled bicarbonate exchanger is involved in the response of iron-responsive element-binding proteins to IVH suggesting a link between the pathogenesis of IVH and ChP ion and iron handling [32]. DFX treatment through chelation of iron may also impact these processes along with normalization of AQP1 ChP protein levels; however, the exact mechanisms of this interaction are unclear and require further investigation [5, 6].

The results of our initial behavioral studies show long-term neurologic injury (sensorimotor reactivity and gating deficits) in rats, although the performance of the HB adolescent rats was not different from that of the CSF group in the majority of behavioral tests. We observed that early DFX treatment had a protective effect against the decreased startle response and chronic sensorimotor gating (PPI response) impairment in the HB group. Homozygous mice with a spontaneous megalencephaly mutation are hypersensitive to acoustic startle, and this condition has negative consequences for synchronous neuronal activity that primes hippocampal networks by increasing their excitability [50]. Moreover,

impaired sensorimotor gating has been related to hippocampal degeneration and volume loss, which have been linked to neonatal IVH [6, 51, 52]. Thus, dysfunctional hippocampal circuitry may be responsible for these behavioral anomalies and be a target for further study. Given the proximity of the hippocampus to the lateral ventricles and the behavioral changes related to a degree of preserved hippocampal function, there may exist a spatial and temporal relationship between the time course of delayed ventriculomegaly and adjacent brain development. It is possible that DFX-mediated early ventricular iron clearance reduced iron-mediated peri-hippocampal injury. Furthermore, these changes likely extend beyond structural damage alone as cortical volumes were similar between HB-injected rats without and with DFX at all time points, and there may be other mechanisms at play such as alteration of CSF and solute circulation in the brain, which could affect these integrated behavioral pathways. It should be noted that we did find some evidence of impairment on one out of six tests within the sensorimotor battery (90° inclined screen) in the HB + DFX rats. However, for reasons outlined in the Supplementary Results, this probably represents a very subtle deficit, but for translational concerns, should be assessed further to determine if it is a reliable finding. Regardless, the inclined screen results of the HB + DFX group are not contradictory relative to the positive effects observed in these rats concerning the sensorimotor reactivity (acoustic startle) and gating (PPI) findings. Specifically, the former task is dependent on the interaction between the somatosensory and motor systems, whereas the latter is dependent on interactions between the auditory and motor systems; and different neural circuits are involved in mediating these functions, which could be differentially affected by the DFX treatment.

Our results show that a single dose of intraventricular DFX at the time of IVH injury is effective in preventing hydrocephalus for up to 11 days in a rat model of neonatal GMH-IVH, with modulation of ChP clearance of iron and solutes, and represents a clinically feasible treatment strategy for preterm IVH. As the prevention of hydrocephalus was limited to 11 days, repeated administration of DFX to produce a more lasting effect may be needed. Importantly, the time-dependent relationship between ChP damage and ChP solute clearance suggests that there exists a finite window in which intraventricular DFX may be effective. The critical role of the ChP in solute clearance and its inherent vulnerability to injury are essential factors to consider in the development of novel treatment options for GMH-IVH/PHH.

4. Materials and Methods

Additional details are provided in the Supplementary Data.

4.1 Animals

All animal procedures were approved and performed according to the Institutional Animal Care and Use Committee (IACUC) of the Washington University School of Medicine protocol #19–0905. Sprague Dawley rats (Charles River Laboratories, Wilmington, MA, USA) were housed with biological mothers and littermates, maintained on a 12-h light/12-h dark daily light cycle, and had access to water, food, and maternal milk ad libitum.

4.2 Intraventricular injections

Surgery was performed on a clean surface with a heating pad. P4 rats were anesthetized using isoflurane (2.5% induction and 1.5% maintenance) then placed prone on a stereotaxic head frame (Stoelting, Wood Dale, IL, USA). Head bars were placed at the external auditory meatus and tightened to minimize head movement. After sterilizing the dorsal cranium, the skull was exposed through a 2.5-mm midline skin incision. Twenty microliters of solution at a 8000-nl/min rate was injected into the right LV (1.5 mm lateral and 0.4 mm anterior to bregma and 2.0 mm deep from the skull surface) using a 30-gauge needle attached to a 0.3-cc syringe held in a micro-infusion pump (World Precision Instruments, Sarasota, FL, USA). The needle was left in place for 5 min then slowly withdrawn to prevent backflow. Incision was closed with 6–0 Ethilon suture (Ethicon Inc, Raritan, NJ, USA). Rats recovered from anesthesia and were returned to their cage with the mother.

4.3 Intraventricular hemorrhage modeling and DFX dose determination

P4 rats were injected with 20 μl aCSF (Tocris Bioscience, Bristol, UK) or HB (EMD Millipore Corp, Burlington, MA, USA) diluted in artificial CSF at 150 mg/ml (equivalent to 3 mg of HB per rat), or HB + DFX with the parameters above. To determine optimal DFX (Sigma-Aldrich, St. Louis, MO, USA) dose, P4 rats were co-injected with different concentrations of DFX (0.4 mg/kg, 1.0 mg/kg, 3.0 mg/kg, 5.0 mg/kg, 10.0 mg/kg, and 20.0 mg/kg, calculated from an average body weight of P4 rat pups i.e.,10 g, mixed in 150 mg/ml HB diluted in aCSF.

4.4 Gold nanoparticle (Au-NP) injections, tissue processing, and imaging

A subset of rats was injected with 20 μl of 1.9 nm Au-NPs (Nanoprobes, Yaphank, NY, USA), diluted in artificial CSF at a 200 mg/ml concentration into the right LV at P7 (72 h after aCSF, HB, or HB + DFX injection at P4). Rats were euthanized 10 min post-AuNP injection via intracardiac perfusion with 10 ml of 1 × phosphate buffered saline (PBS) followed by 10 ml of 4% paraformaldehyde (PFA) (ThermoFisher scientific, Waltham, MA, USA). After perfusion, brains were removed, washed with 1 × PBS for 3 h, and processed through alcohol grades (30%, 50%, and 70% ethanol for 30 min each) before fixing into paraffin and embedding. Brains were subsequently coronally sectioned at 7–10-μm thickness using a Leica microtome (Leica Microsystems, Wetzlar, Germany). Sections were deparaffinized and mounted using xylene-based mounting medium (Cytoseal XYL, ThermoFisher scientific, Waltham, MA, USA). The integrated density of AuNPs was measured at five random areas of a single frame of ChP for a minimum of six images per rat (n = 4/group), and the background was subtracted to calculate the mean integrated density value. All image quantifications were performed using the ImageJ software (version: 2.1.0/1.53C) [53].

4.5 Histology and hematoxylin and eosin (H&E) staining

After deparaffinization and hydration, sections were stained with hematoxylin for 1 min then eosin for 3 min with intermittent rinsing in tap water for 5 min. After dehydration in ascending grades of alcohol (70%, 95%, 100%) and xylene (20 min), sections were mounted

using a xylene-based mounting medium (Cytoseal XYL, ThermoFisher scientific, Waltham, MA, USA) and imaged using a Leica microscope (Leica Microsystems, Wetzlar, Germany).

4.6 Determination of ependymal and ChP injury

H&E-stained images were used to evaluate ependymal and ChP injury. The length of non-intact or perturbed ependymal regions on the lateral wall of a single frame per rat (n = 4/ group) was measured and divided by the total perimeter of the wall of the LV to determine ependymal injury. To assess the integrity of the ChP, epithelial cells that were separated from the intact ChP epithelium and the total number of ChP cells were counted. Injured ChP cell percentage was calculated by the number of non-intact ChP cells divided by the total number of ChP cells. ChP luminal diameter was measured across a single layer of apical cells and the lumen at 20 random areas of the ChP of a single frame per rat (n = 4/ group). The total luminal measurements of intact regions of ChP were averaged to obtain the mean ChP diameter per rat.

4.7 Immunofluorescence

Deparaffinized brain sections were quenched in hydrogen peroxide and methanol (1 ml/200 ml respectively) for 20 min at room temperature. Antigen retrieval was performed using Diva Decloaker Solution (Biocare Medical, Concord, CA, USA) for 2 min at 120 °C and 30 s at 90 °C in a lab-rated pressure cooker (Dako Cytomation, Glostrup, Denmark). Once cooled to room temperature, sections were blocked using 5% bovine serum albumin (Sigma-Aldrich, St. Louis, MO, USA) in 1 × PBS and 1% Triton X-100 (TX-100) (Sigma-Aldrich, St. Louis, MO, USA). Sections were then incubated separately with primary antibodies to the following proteins (AQP1 1:100 (Mouse, ab9566, Abcam, Cambridge, UK), NKCC1 1:100 (Rabbit, ab59791, Abcam, Cambridge, UK), and NKAT 1:50 (Rabbit, ab76020, Abcam, Cambridge, UK) overnight at 4 °C. Slides were washed six times for 5 min each with 1 × PBS-TX-100 and incubated for 1 h with respective anti-rabbit (A32731, ThermoFisher scientific, Waltham, MA, USA) or anti-mouse (A32723, ThermoFisher scientific, Waltham, MA, USA) 488 Alexa fluor conjugated secondary antibodies (1:2000). Slides were washed six times for 5 min each with 1 × PBS-TX-100, and mounted with ProLong™ Gold Antifade with 4′,6-diamidino-2-phe-nylindole (DAPI) (ThermoFisher scientific, Waltham, MA, USA). The fluorescent sections were imaged using a Leica microscope (Leica Microsystems, Wetzlar, Germany) or a Hamamatsu NanoZoomer microscope (2.0-HT System, Hamamatsu City, Japan) to visualize protein localization and expression. Mean fluorescent intensities for AQP1, NKCC1, and NKAT were calculated from six random regions of ChP per frame (3–4 frames per rat), and the background was subtracted from the total intensity to calculate the mean intensity of LV ChP per rat.

4.8 Terminal deoxynucleotidyl transferase deoxyuridine triphosphate nick end labeling (TUNEL) assay

TUNEL assay was performed to detect DNA fragmentation in the epithelial cells of the ChP. After sections were deparaffinized, sections were stained as per the manufacturer's protocol (Millipore-Sigma, St. Louis, MO, USA) and counterstained with DAPI. The percentage of TUNELpositive cells was determined by counting the number of TUNEL-positive cells (green) divided by the total number of DAPI-positive ChP cells (blue). Six random images

of the ChP per rat were analyzed to determine the percent of TUNEL-positive cells in the ChP for each rat (n = 3–6/ group).

4.9 Perls iron staining

Perls Prussian blue staining was performed as per manufacturer's protocol (HT20–1KT, Sigma-Aldrich, St. Louis, MO, USA) with slight modifications. Briefly, paraffin-embedded and rehydrated brain sections were stained with Perls solution for 7 min, counterstained with nuclear fast red for 2 min, and rinsed intermittently in running tap water for 5 min. Sections were dehydrated using alcohol grades (30%, 50%, 70%, 95%, 100% for 5 min each) and xylene (20 min) as above and embedded with xylene-based mounting medium (Cyto-seal XYL, ThermoFisher scientific, Waltham, MA, USA). Images were obtained of the ChP from the right and left LVs, cortex, hippocampus, and periventricular ependyma at 6 h, 24 h, 72 h, and 11 days after injection to determine the time course of iron (Fe3+) clearance in the ChP (Leica Microsystems, Wetzlar, Germany). The integrated density of blue staining was measured at six random areas of a single frame of ChP for a minimum of six images per rat (n = 3/group), and background was subtracted to calculate the mean integrated density.

4.10 MRI and brain volume measurements

To determine ventricle and brain cortex volumes, T2-weighted MRIs were acquired at 72 h, 17 days (P21), and 56 days (P60) post-injection using a 4.7 T Varian MRI scanner (Varian Inc., Palo Alto, CA, USA). Rats were anesthetized using isoflurane (2.5% induction, 1.5% maintenance) and kept warm using a heated air blower. T2-weighted fast spin echo sequences (repetition time 3000/echo time 27.50 ms, four averages, field of view 18.0 mm × 18.0 mm, matrix 128 × 128, 24 axial slices, and 0.50 mm thick) were used to acquire images. T2-weighted MRIs at 11 days post-injection (P15) were acquired using a 9.4 T Bruker MRI scanner (Bruker, MA, USA) with T2-weighted fast spin echo sequences (repetition time = 5000 ms, echo time = 66.00 ms, echo spacing = 16.50 ms, number of averages = 2, repetitions = 1, rare factor = 8, field of view = 16.0 mm × 16.0 mm, matrix = 256 × 256, number of axial slices = 32, thickness = 0.50 mm). The ventricles (left LV, right LV, 3V, and 4V), CSP (defined as the CSF space medial to the LVs and rostral to the 3V [54], and cortex were manually segmented on coronal images using ITK-SNAP software (version 3.8.0), and volumes were calculated by multiplying slice thickness by segmented area on each slice and then summing across slices. Ventricular volumes were calculated by manual segmentation of T2 hyperintense spaces. 3D images of the ventricles were automatically rendered following segmentation. Cortical volumes were calculated by manual segmentation of the grey matter between the corpus callosum or external capsule and the cortical surface from the prefrontal cortex to the visual cortex. All segmentations were performed with cross-reference to an anatomical atlas [55].

Fisher's exact test was used to compare rates of hydrocephalus between HB and HB + DFX conditions at P7 and P15, and aCSF and HB conditions at P7, P21, and P60. Hydrocephalus in all analyses was defined as ventricle volumes greater than three standard deviations above the mean of aCSF-injected animals [30]. 0.5 was added to each value before calculating the relative risk to avoid dividing by zero, as zero aCSF and HB + DFX animals developed

hydrocephalus. All tests were two-tailed, and a p value of less than 0.05 was considered significant. Data were analyzed using GraphPad Prism version 9.3.1 (350).

4.11 Behavioral studies

Behavioral testing began on P28 for each group (CSF, HB, and HB + DFX (n = 9 each)) and ended on P46. Testing was conducted by individuals blinded to treatment. The tests were conducted in the following sequence: open-field, a battery of sensorimotor measures, EPM, acoustic startle and PPI, and the MWM. These tests were adapted from standard tests used with adult rodents to make them appropriate for adolescent rats [56, 57]. A detailed description of the methodology and timeline for each test and specific references are provided in the Supplementary Methods.

4.12 Statistics

Statistical analysis was performed using the Prism software (Version 7.0). Data were analyzed using Student's t test, Fisher's exact test, and one-way ANOVA with Tukey's post-hoc test for multiple comparisons. All data shown in histograms were mean ± standard error of the mean (SEM). $p < 0.05$ was considered statistically significant. Analysis of the behavioral data included repeated measures ANOVA models, which are described in detail in the Supplementary Methods.

Supplementary Material

Refer to Web version on PubMed Central for supplementary material.

Acknowledgements

The studies presented in this work were carried out, in part, using the Small Animal MR Facility of the Mallinckrodt Institute of Radiology, Hope Center Alafi Neuroimaging Lab, and Washington University Center for Cellular Imaging (WUCCI), supported by Washington University in St. Louis School of Medicine.

Funding

NIH R01 NS110793 (JMS), K12 Neurosurgeon Research Career Development Program (JMS), Hydrocephalus Association (JMS), WUCCI, McDonnell Centers for Systems Neuroscience and Cellular Neurobiology (JMS, DFW), Children's Discovery Institute of Washington University and St. Louis Children's Hospital (JMS). The MRI studies presented in this work were carried out in the Small Animal MR Facility of the Mallinckrodt Institute of Radiology at Washington University (18-019, JMS).

Data availability

The data that support the findings of this study may be available at the discretion of the corresponding author, upon reasonable request.

Abbreviations

GMH	germinal matrix hemorrhage
IVH	intraventricular hemorrhage
HB	hemoglobin

DFX	deferoxamine
PHH	posthemorrhagic hydrocephalus
ChP	choroid plexus
LV	lateral ventricle
AuNP	gold nanoparticle
PBS	phosphate buffered saline
PFA	paraformaldehyde
H&E	hematoxylin and eosin
AQP1	aquaporin-1
NKAT	sodium potassium ATPase
NKCC1	sodium potassium chloride cotransporter
DAPI	4′,6-diamidino-2-phenylindole
TUNEL	terminal deoxynucleotidyl transferase deoxyuridine triphosphate nick end labeling
EPM	elevated plus maze
PPI	prepulse inhibition
MWM	Morris water maze
SEM	standard error of the mean
rm	repeated measures
CSP	cavum septum pellucidum

References

1. Ballabh P Intraventricular hemorrhage in premature infants: mechanism of disease. Pediatr Res. 2010;67(1):1–8. [PubMed: 19816235]
2. Strahle JM, Triplett RL, Alexopoulos D, Smyser TA, Rogers CE, Limbrick DD, et al. Impaired hippocampal development and out-comes in very preterm infants with perinatal brain injury. NeuroImage Clinical. 2019;22:101878.
3. Christian EA, Melamed EF, Peck E, Krieger MD, McComb JG. Surgical management of hydrocephalus secondary to intraventricular hemorrhage in the preterm infant. J Neurosurg Pediatr. 2016;17(3):278–84. [PubMed: 26565942]
4. Gao C, Du H, Hua Y, Keep RF, Strahle J, Xi G. Role of red blood cell lysis and iron in hydrocephalus after intraventricular hemorrhage. J Cereb Blood Flow Metab. 2014;34(6):1070–5. [PubMed: 24667910]
5. Garton T, Keep RF, Hua Y, Xi G. Brain iron overload following intracranial haemorrhage. Stroke Vasc Neurol. 2016;1(4):172–84. [PubMed: 28959481]

6. Garton TP, He Y, Garton HJL, Keep RF, Xi G, Strahle JM. Hemoglobin-induced neuronal degeneration in the hippocampus after neonatal intraventricular hemorrhage. Brain Res. 2016;1635:86–94. [PubMed: 26772987]
7. Mahaney KB, Buddhala C, Paturu M, Morales D, Limbrick DD, Strahle JM. Intraventricular hemorrhage clearance in human neonatal cerebrospinal fluid: associations with hydrocephalus. Stroke. 2020;51(6):1712–9. [PubMed: 32397930]
8. Strahle JM, Garton T, Bazzi AA, Kilaru H, Garton HJL, Maher CO, et al. Role of hemoglobin and iron in hydrocephalus after neonatal intraventricular hemorrhage. Neurosurg. 2014;75(6):696–706.
9. Strahle JM, Mahaney KB, Morales DM, Buddhala C, Shannon CN, Wellons JC, et al. Longitudinal CSF iron pathway proteins in posthemorrhagic hydrocephalus: associations with ventricle size and neurodevelopmental outcomes. Annal Neurol. 2021;90:2.
10. Ballabh P, de Vries LS. White matter injury in infants with intraventricular haemorrhage: mechanisms and therapies. Nature Rev Neurol. 2021;17(4):199–214. [PubMed: 33504979]
11. Merhar SL, Tabangin ME, Meinzen-Derr J, Schibler KR. Grade and laterality of intraventricular haemorrhage to predict 18–22 month neurodevelopmental outcomes in extremely low birthweight infants. Acta Paediat Intl J Paediatr. 2012;101(4):414–8.
12. Murphy BP, Inder TE, Rooks V, Taylor GA, Anderson NJ, Mogridge N, et al. Posthaemorrhagic ventricular dilatation in the premature infant: natural history and predictors of outcome. Arch Dis Child Fetal Neonatal Edit. 2002;87(1):37F – 41.
13. Volpe JJ. Brain injury in premature infants: a complex amalgam of destructive and developmental disturbances. Lancet Neurol. 2009;8(1):110–24. [PubMed: 19081519]
14. Cherian SS, Love S, Silver IA, Porter HJ, Whitelaw AGL, Thoresen M. Posthemorrhagic ventricular dilation in the neonate: development and characterization of a rat model. J Neuropathol Exp Neurol. 2003;62(3):292–303. [PubMed: 12638733]
15. Wan S, Hua Y, Keep RF, Hoff JT, Xi G. Deferoxamine reduces CSF free iron levels following intracerebral hemorrhage. Acta Neurochir Suppl. 2006;96:199–202. [PubMed: 16671454]
16. Gozzelino R, Arosio P. Iron homeostasis in health and disease. Intl J Mol Sci. 2016;17(1):130.
17. Klebe D, Krafft PR, Hoffmann C, Lekic T, Flores JJ, Rolland W, et al. Acute and delayed Deferoxamine treatment attenuates long-term sequelae after germinal matrix hemorrhage in neonatal rats. Stroke. 2014;45(8):2475–9. [PubMed: 24947291]
18. LeBlanc RH, Chen R, Selim MH, Hanafy KA. Heme oxygenase1-mediated neuroprotection in subarachnoid hemorrhage via intracerebroventricular deferoxamine. J. Neuroinflammation 2016;13(1):244. [PubMed: 27618864]
19. Lekic T, Klebe D, Pichon P, Brankov K, Sultan S, McBride D, et al. Aligning animal models of clinical germinal matrix hemorrhage, from basic correlation to therapeutic approach. Curr. Drug Targets 2016;18(12):1316–1328.
20. Mackenzie EL, Iwasaki K, Tsuji Y. Intracellular iron transport and storage: from molecular mechanisms to health implications. Antioxid. Redox Signaling 2008;10(6):997–1030.
21. Meng H, Li F, Hu R, Yuan Y, Gong G, Hu S, et al. Deferoxamine alleviates chronic hydrocephalus after intraventricular hemorrhage through iron chelation and Wnt1/Wnt3a inhibition. Brain Res. 2015;1602(44):52.
22. Mobarra N, Shanaki M, Ehteram H, Nasiri H, Sahmani M, Saeidi M, et al. A review on iron chelators in treatment of iron overload syndromes. Int J Hematol Oncol Stem Cell Res. 2016;10(4):239–247. [PubMed: 27928480]
23. Phaniendra A, Jestadi DB, Periyasamy L. Free radicals: properties, sources, targets, and their implication in various diseases. Indian J Clin Biochem. 2015;30(1):11–26. [PubMed: 25646037]
24. Sun A, Wang J. Choroid plexus and drug removal mechanisms. AAPS Journal. 2021;23(3):61. [PubMed: 33942198]
25. Zhang DL, Ghosh MC, Rouault TA. The physiological functions of iron regulatory proteins in iron homeostasis—an update. Front. Pharmacol 2014;5:124. [PubMed: 24982634]
26. Chen Q, Tang J, Tan L, Guo J, Tao Y, Li L, et al. Intracerebral hematoma contributes to hydrocephalus after intraventricular hemorrhage via aggravating iron accumulation. Stroke. 2015;46(10):2902–8. [PubMed: 26265129]

27. Zhang J, Shi X, Chen Z, Geng J, Wang Y, Feng H, et al. Edaravone reduces iron-mediated hydrocephalus and behavioral disorder in rat by activating the Nrf2/HO-1 pathway. J. Stroke Cerebrovasc Dis 2018;27(12):3511–3520. [PubMed: 30205995]
28. Dang S, Rasmussen CA, LeVine SM. Immunocytochemical localization of desferrioxamine in the kidney, liver and brain of the developing and adult mouse: implications for drug processing and therapeutic mechanisms. Res Commun Mol Pathol Pharmacol. 1994 Oct;86(1):43–57. [PubMed: 7850256]
29. Xu H, Fame RM, Sadegh C, Sutin J, Naranjo C, della Syau, et al. Choroid plexus NKCC1 mediates cerebrospinal fluid clearance during mouse early postnatal development. Nat Commun 2021;12(1):447 [PubMed: 33469018]
30. Okubo S, Strahle J, Keep RF, Hua Y, Xi G. Subarachnoid hemorrhage-induced hydrocephalus in rats. Stroke. 2013;44(2):547–550. [PubMed: 23212164]
31. Klebe D, McBride D, Krafft PR, Flores JJ, Tang J, Zhang JH. Pos-themorrhagic hydrocephalus development after germinal matrix hemorrhage: established mechanisms and proposed pathways. J Neurosci Res. 2020;98(1):105–120. [PubMed: 30793349]
32. Li Q, Ding Y, Krafft P, Wan W, Yan F, Wu G, et al. Targeting germinal matrix hemorrhage-induced overexpression of sodium-coupled bicarbonate exchanger reduces Posthemorrhagic hydrocephalus formation in neonatal rats. J Am Heart Assoc. 2018;7(3):e007192. [PubMed: 29386206]
33. Semple BD, Blomgren K, Gimlin K, Ferriero DM, Noble-Haeusslein LJ. Brain development in rodents and humans: identifying benchmarks of maturation and vulnerability to injury across species. Prog. Neurobiol 2013;106–107:1–16. [PubMed: 24012715]
34. Ding Y, Zhang T, Wu G, McBride DW, Xu N, Klebe DW, et al. Astrogliosis inhibition attenuates hydrocephalus by increasing cerebrospinal fluid reabsorption through the glymphatic system after germinal matrix hemorrhage. Exp Neurol. 2019;320:113003. [PubMed: 31260658]
35. Gao F, Liu F, Chen Z, Hua Y, Keep RF, Xi G. Hydrocephalus after intraventricular hemorrhage: the role of thrombin. J Cereb. Blood Flow Metab 2014;34(3):489–494. [PubMed: 24326390]
36. Longatti PL, Basaldella L, Orvieto E, Fiorindi A, Carteri A. Choroid plexus and aquaporin-1: a novel explanation of cerebrospinal fluid production. Pediatr Neurosurg. 2004;40(6):277–83. [PubMed: 15821358]
37. Strahle J, Garton HJL, Maher CO, Muraszko KM, Keep RF, Xi G. Mechanisms of hydrocephalus after neonatal and adult intraventricular hemorrhage. Transl. Stroke Res 2012;(Suppl 1):25–38.
38. Rouault TA, Zhang DL, Jeong SY. Brain iron homeostasis, the choroid plexus, and localization of iron transport proteins. Metab Brain Dis. 2009;24(4):673–684. [PubMed: 19851851]
39. Alvira-Botero X, M. Carro E. Clearance of amyloid-β peptide across the choroid plexus in Alzheimers disease. Curr. Aging Sci 2010;3(3):219–29. [PubMed: 20735345]
40. Ogawa M, Suzuki H, Sawada Y, Hanano M, Sugiyama Y. Kinetics of active efflux via choroid plexus of β-lactam antibiotics from the CSF into the circulation. Am J Physiol Regul Integr Comp Physiol. 1994;266(2 Pt 2):R392–9.
41. Schweizer C, Fraering PC, Kühn LC. Ferritin H gene deletion in the choroid plexus and forebrain results in hydrocephalus. Neurochem Int. 2014;71:17–21. [PubMed: 24662374]
42. Eide PK, Valnes LM, Pripp AH, Mardal KA, Ringstad G. Delayed clearance of cerebrospinal fluid tracer from choroid plexus in idiopathic normal pressure hydrocephalus. J. Cereb. Blood Flow Metab 2020;40(9):1849–1858. [PubMed: 31495299]
43. Tadayon E, Pascual-Leone A, Press D, Santarnecchi E. Choroid plexus volume is associated with levels of CSF proteins: relevance for Alzheimer's and Parkinson's disease. Neurobiol Aging. 2020;89:108–117 [PubMed: 32107064]
44. Ghaffari H, Grant SC, Petzold LR, Harrington MG. Regulation of CSF and brain tissue sodium levels by the blood-CSF and blood-brain barriers during migraine. Front Comput Neurosci. 2020;14:4. [PubMed: 32116618]
45. Karimy JK, Zhang J, Kurland DB, Theriault BC, Duran D, Sto-kum JA, et al. Inflammation-dependent cerebrospinal fluid hyper-secretion by the choroid plexus epithelium in posthemorrhagic hydrocephalus. Nat Med. 2017 Aug;23(8):997–1003. [PubMed: 28692063]

46. Johanson CE, Duncan JA, Klinge PM, Brinker T, Stopa EG, Silverberg GD. Multiplicity of cerebrospinal fluid functions: new challenges in health and disease. Cerebrospinal Fluid Research. 2008;5:10. [PubMed: 18479516]
47. Castañeyra-Ruiz L, Hernández-Abad LG, Carmona-Calero EM, Castañeyra-Perdomo A, González-Marrero I. AQP1 overexpression in the CSF of obstructive hydrocephalus and inversion of its polarity in the choroid plexus of a Chiari malformation type II case. J Neuropathol Exp Neurol. 2019;78(7):641–647. [PubMed: 31039249]
48. Casey JL, Koeller DM, Ramin VC, Klausner RD, Harford JB. Iron regulation of transferrin receptor mRNA levels requires iron-responsive elements and a rapid turnover determinant in the 3' untranslated region of the mRNA. EMBO Journal. 1989;8(12):3693–3699. [PubMed: 2583116]
49. Hentze MW, Caughman SW, Rouault TA, Barriocanal JG, Dancis A, Harford JB, et al. Identification of the iron-responsive element for the translational regulation of human ferritin mRNA. Science. 1987;238(4833):1570–3. [PubMed: 3685996]
50. Fisahn A, Lavebratt C, Canlon B. Acoustic startle hypersensitivity in Mceph mice and its effect on hippocampal excitability. Eur J Neurosci. 2011;34(7):1121–30. [PubMed: 21966978]
51. Rezayat M, Roohbakhsh A, Zarrindast MR, Massoudi R, Dja-hanguiri B. Cholecystokinin and GABA interaction in the dorsal hippocampus of rats in the elevated plus-maze test of anxiety. Physiol Behav. 2005;84(5):775–82. [PubMed: 15885255]
52. Swerdlow NR, Light GA, Breier MR, Shoemaker JM, saint Marie RL, Neary AC, et al. Sensory and sensorimotor gating deficits after neonatal ventral hippocampal lesions in rats. Dev Neurosci. 2012;34(2–3):240–9. [PubMed: 22572564]
53. Schindelin J, Arganda-Carreras I, Frise E, Kaynig V, Longair M, Pietzsch T, et al. Fiji: an open-source platform for biological-image analysis. Nat Methods. 2012;9(7):676–82. [PubMed: 22743772]
54. Kaur C, Ling EA. Transitory cystic cavities in the developing mammalian brain – normal or anomalous? Journal of Anatomy. 2017;230(2):197–202. [PubMed: 27761896]
55. Paxinos G, Watson C. The rat brain in stereotaxic coordinates seventh edition. Elsevier Academic Press. 2014;170.
56. Maloney SE, Yuede CM, Creeley CE, Williams SL, Huffman JN, Taylor GT, et al. Repeated neonatal isoflurane exposures in the mouse induce apoptotic degenerative changes in the brain and relatively mild long-term behavioral deficits. Sci Rep. 2019;9(1):2779. [PubMed: 30808927]
57. Palanisamy A, Giri T, Jiang J, Bice A, Quirk JD, Conyers SB, et al. In utero exposure to transient ischemia-hypoxemia pro-motes long-term neurodevelopmental abnormalities in male rat offspring. JCI Insight. 2020;5(10):e133172. [PubMed: 32434985]

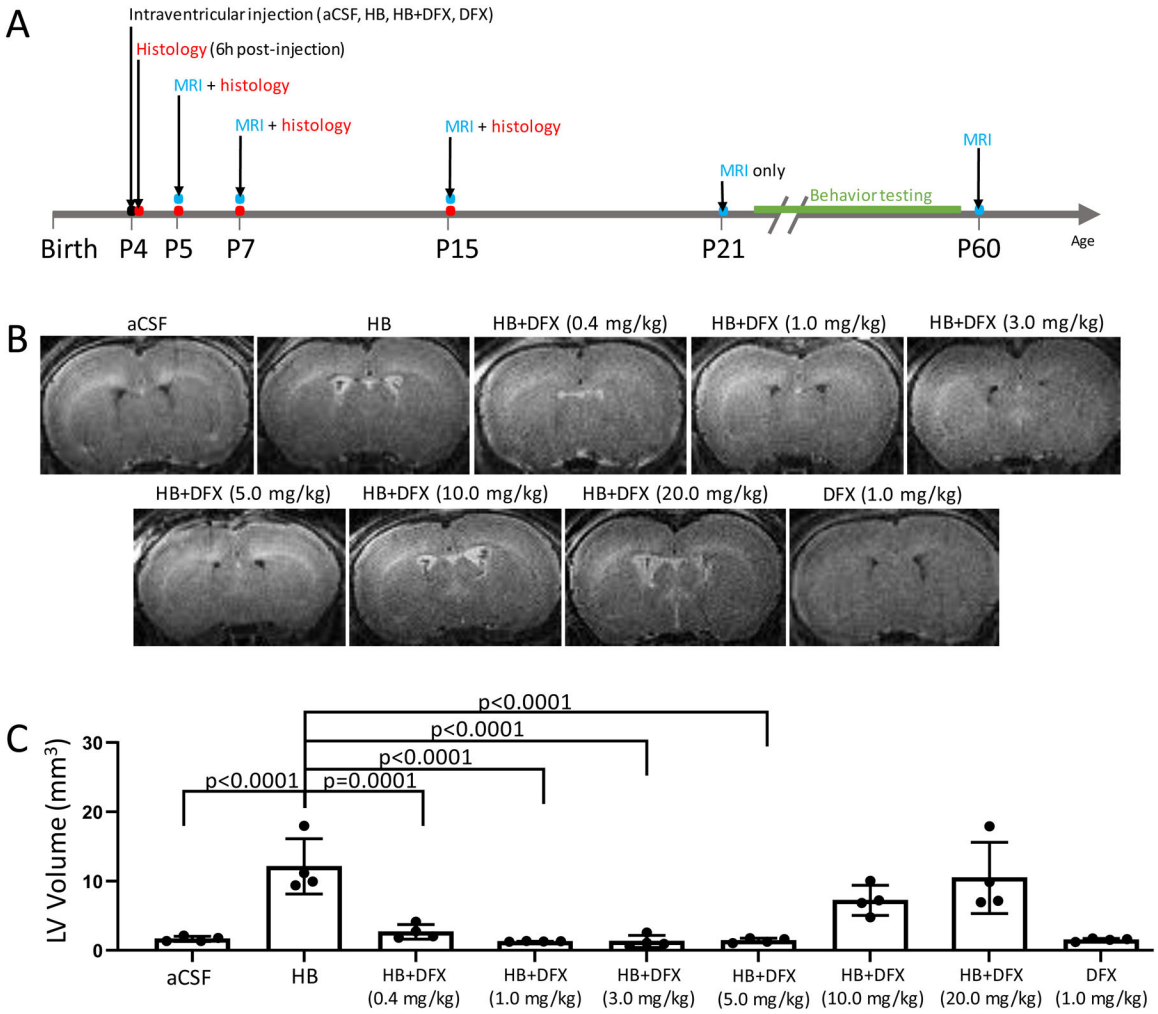

Fig. 1. Dose-dependent effect of intraventricular deferoxamine (DFX) administered at the time of hemorrhage on the development of posthemorrhagic hydrocephalus.

(A) Timeline of experimental plan. Artificial CSF (aCSF), hemoglobin (HB), HB + DFX, or DFX only were injected into the right lateral ventricle at post-natal day 4 (P4). Rats were either sacrificed 6 h, 24 h (at P5), 72 h post-injection (at P7), or 11 days post-injection (at P15) for histology, and underwent T2-weighted MRI at P5, P7, and P15 prior to sacrifice. A separate cohort of rats were followed longitudinally and underwent MRI scans at P7, P21, and P60 to assess ventricle volume and behavioral testing from P28 to P46. Histology time points are shown in red, MRI in blue, and behavioral testing in green. (B) Representative T2-weighted MRI images of the brain showing the effect of 20 μL aCSF, HB (150 mg/mL), and HB + DFX, with DFX treatment doses ranging from 0.4 to 20.0 mg/kg. The effect of 1.0 mg/kg DFX only injection is also shown. All MRIs shown were performed 72 h post-injection. (C) Quantification of lateral ventricle volumes 72 h post-injection. Data are mean ± SEM, n = 4 per group; one-way ANOVA with post-hoc Tukey test.

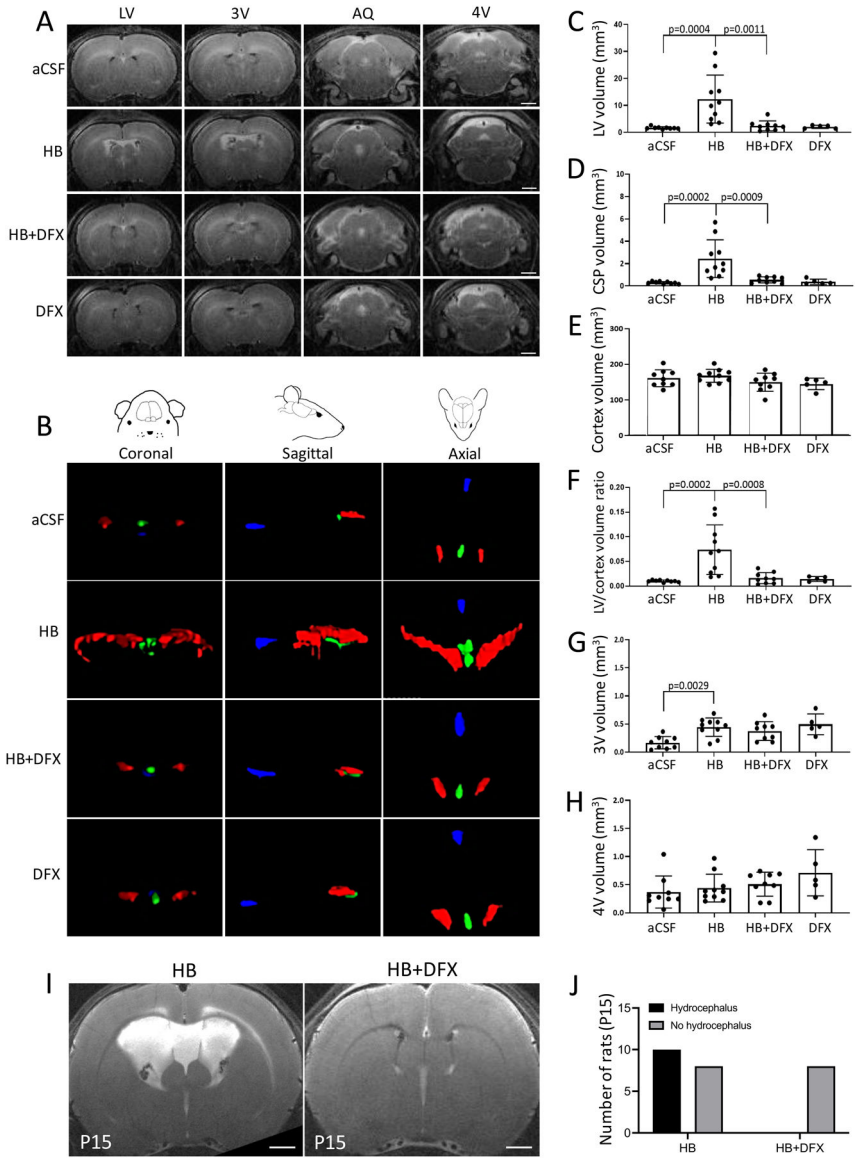

Figure 2. Deferoxamine (DFX) treatment at the time of hemorrhage prevents region-specific ventricular expansion after neonatal intra-ventricular hemorrhage (IVH).

(A) Representative T2-weighted MRI images showing the lateral ventricles (LV), 3rd ventricle (3V), cerebral aqueduct (AQ), and 4th ventricle (4V) 72 h post-intraventricular injection of artificial CSF (aCSF), hemoglobin (HB), HB + DFX, or DFX in post-natal day 4 rats. Scalebars = 1 mm. (B) 3D reconstructions of the ventricular system (LV red, 3V green, 4V blue) 72 h post-injection in the axial, sagittal, and coronal planes. (C–H) Quantification of LV (C), cavum septum pellucidum (CSP) (D), cortex (E), LV/cortex ratio (F), 3V (G), and 4V (H) volumes 72 h post-injection. HB injection resulted in significant increases in LV, CSP, and 3V volumes, as well as an increase in the LV/cortex ratio, but no significant differences in cortex or 4V volumes. DFX treatment at the time of IVH induction resulted in significantly smaller LV and CSP volumes compared to rats injected with HB only. Data are mean ± SEM, n = 9–10 per group; one-way ANOVA with post-hoc Tukey test. (I–J) The rate of hydrocephalus in HB + DFX-injected rats (0 of 8) was significantly lower than the rate of

hydrocephalus in HB animals (10 of 18) 11 days post-injection at P15. scalebar = 1 mm. p = 0.0095, Fisher's exact test

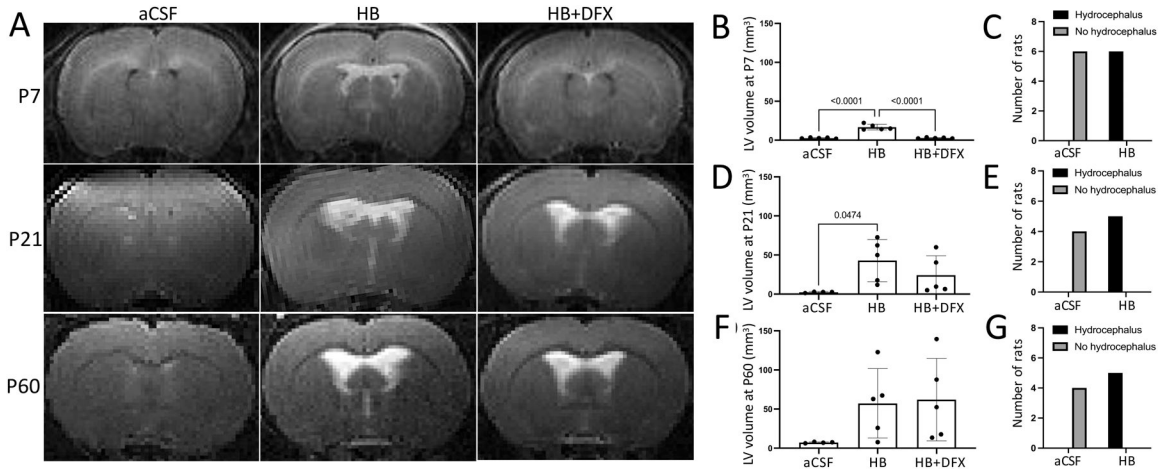

Figure 3. Deferoxamine (DFX) treatment prevents acute, but not chronic hydrocephalus after IVH.

(A) Representative T2-weighted MRIs at postnatal day 7 (P7), P21, and P60 after intraventricular injection of artificial CSF (aCSF), hemoglobin (HB), or HB + deferoxamine (HB+DFX) at P4. (B–C) Quantification of lateral ventricle (LV) volume (B) and rate of hydrocephalus development (C) at P7. (D–E) Quantification of LV volume (D) and rate of hydrocephalus development (E) at P21. (F–G) Quantification of LV volume (F) and rate of hydrocephalus development (G) at P60. Lateral ventricle volume data are mean ± SEM, n = 4–5 per group; one-way ANOVA with post-hoc Tukey test. Hydrocephalus data are analyzed with Fisher's exact test

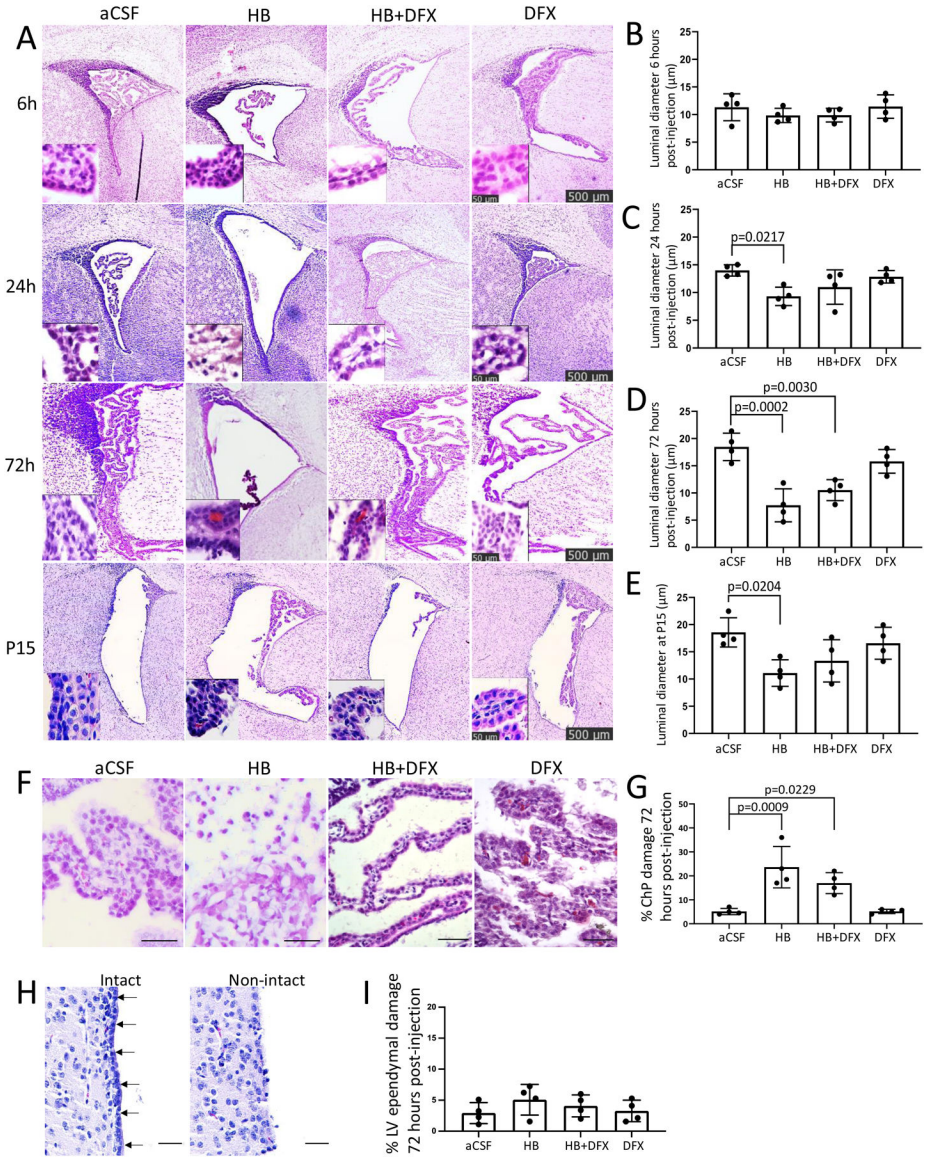

Figure 4. Selective choroid plexus (ChP) injury in the lateral ventricles (LV) after neonatal intraventricular hemorrhage is not prevented by deferoxamine (DFX).

(A) Representative hematoxylin and eosin (H&E) images of the LVs 6 h, 24 h (P5), 72 h (P7), and 11 days (P15) after intraventricular injection of aCSF, hemoglobin (HB), HB + DFX, or DFX alone in post-natal day 4 (P4) rats. Insets highlight ChP structure. Scalebars = 500 µm, inset scalebars = 50 µm. (B–E) Quantification of ChP luminal diameter 6 h (B), 24 h (C), 72 h (D), and 11 days (P15) (E) after aCSF, HB, HB + DFX, or DFX injection at P4. The luminal diameter in HB-injected rats is significantly decreased at 24 h (C), 72 h (D), and at P15 (E) compared to aCSF-injected rats. HB-induced decreases in ChP luminal diameters were variably affected by DFX treatment, with no significant differences between the HB and HB+DFX groups at any timepoint. Data are mean ± SEM, n = 4 per group; one-way ANOVA with post-hoc Tukey test. (F–G) Representative H&E images (F) and quantification (G) of ChP injury 72 h after intraventricular aCSF, HB, HB + DFX, or DFX injection. (H–I) Representative H&E images of intact (arrows) and non-intact LV ependyma (H) with

quantification of LV ependymal injury 72 h after intraventricular injection of aCSF, HB, HB + DFX, or DFX alone (I). Scale bars = 50 μm. Data are mean ± SEM, n = 4 per group; one-way ANOVA with post-hoc Tukey test

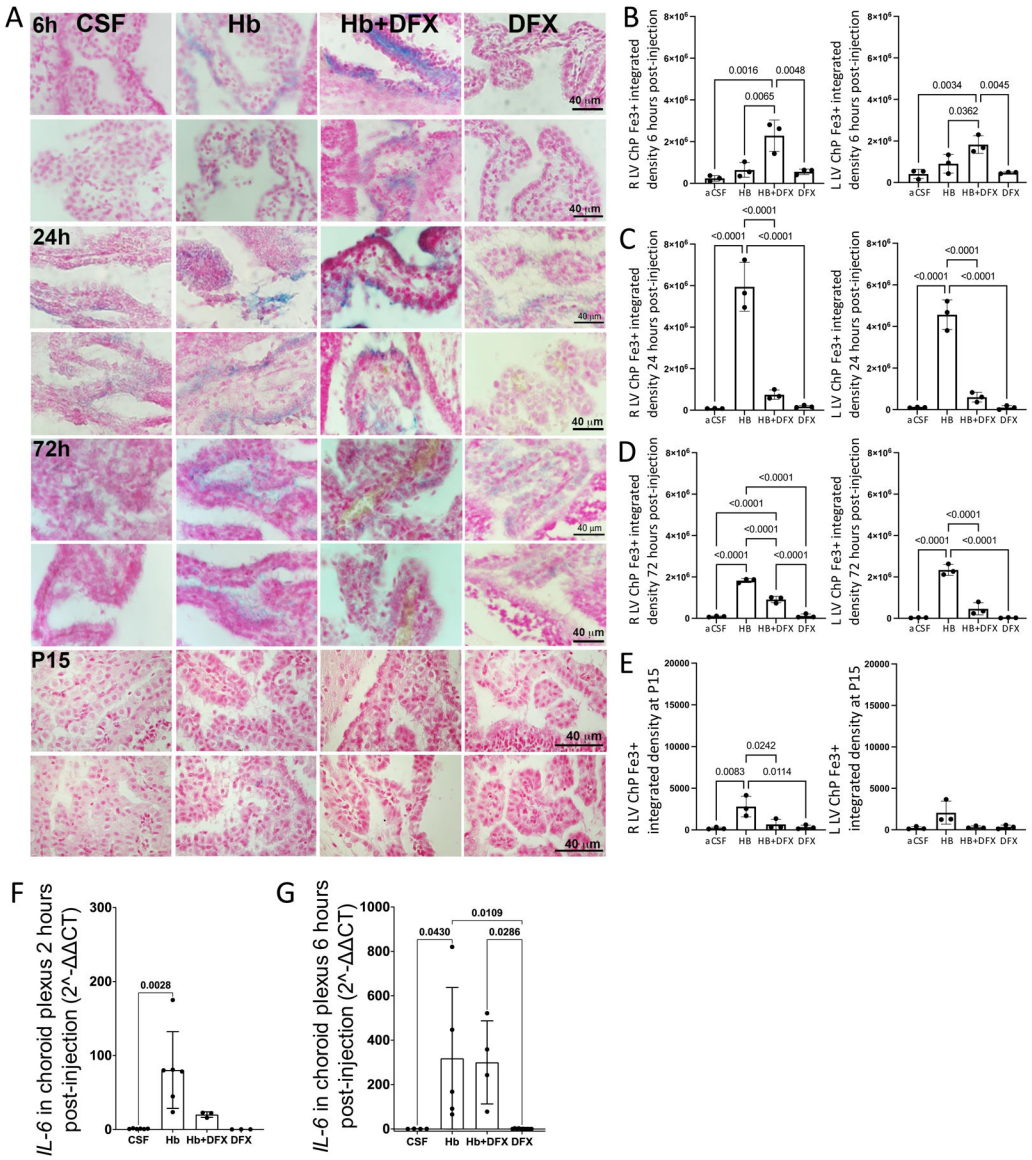

Figure 5. Early deferoxamine (DFX)-mediated iron clearance through the choroid plexus (ChP).

(A) Early deferoxamine (DFX)-mediated iron clearance through the choroid plexus (ChP). (A) Representative images of Perls iron staining (blue) in the lateral ventricle (LV) ChP 6 h, 24 h, 72 h, and 11 days (P15) after intraventricular injection of artificial CSF (aCSF), hemoglobin (HB), HB + DFX, or DFX alone in post-natal day 4 rats. For each time point, the top row is the right LV and bot-tom is the left LV. At 6 h post-injection, ChP iron was found primarily in the lumen in the HB + DFX group, while iron was present in the ChP epithelium in other groups. (B–E) Quantification of ChP iron in the right and left LVs at 6 h (B), 24 h (C), 72 h (D), and 11 days (P15) (E) post-injection. There was increased iron accumulation at 24 h, 72 h, and 11 days (P15) after HB injection compared to aCSF controls. HB + DFX-injected rats had significantly more iron within the ChP compared to aCSF controls at 6 h post-injection (B), and demonstrated a reduced iron burden within the ChP at 24 h (C), 72 h (D), and 11 days (P15) (E) compared to the HB group. Data are mean

± SEM, n = 3 per group; one-way ANOVA with post-hoc Tukey test. (F-G) Choroid plexus RNA levels of IL-6 determined by qRT-PCR 2 h and 6 h post-intraventricular hemorrhage (IVH) induction (HB injection), normalized to β-actin. Quantification showed increased IL-6 expression at 2 h and 6 h post-IVH. DFX treatment resulted in a trend towards decreased IL-6 expression at the 2-h time-point. Data are mean ± SEM, n = 3 per group; one-way ANOVA with post-hoc Tukey test

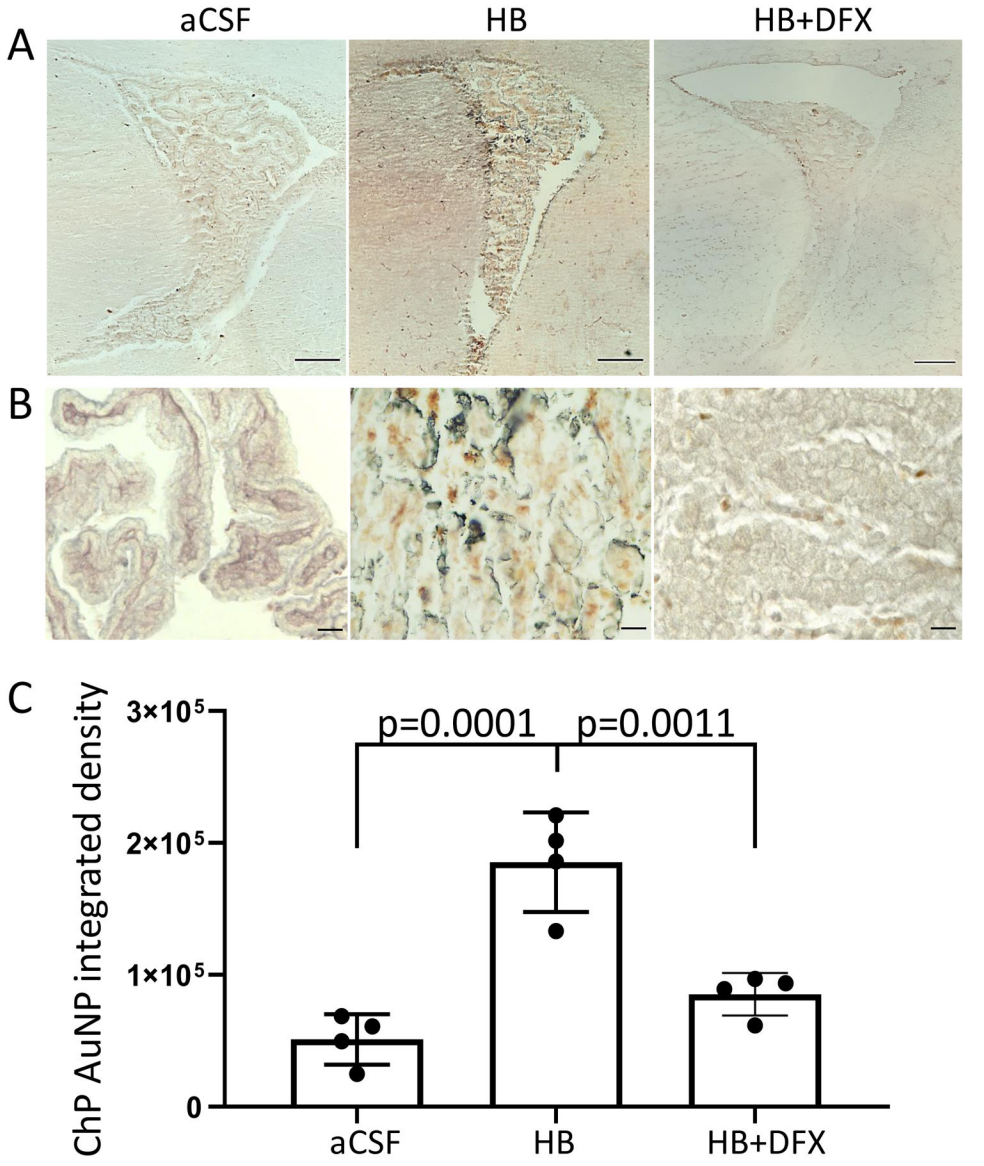

Figure 6. Iron-mediated choroid plexus (ChP) dysfunction after intraventricular hemorrhage results in reduced CSF solute clearance.

(A-B) Iron-mediated choroid plexus (ChP) dysfunction after intraventricular hemorrhage results in reduced CSF solute clearance. (A–B) Representative photomicrographs of the right lateral ventricle (LV) (A) and right LV ChP (B) 10 min after intraventricular injection of 1.9-nm gold nanoparticles (AuNPs) 72 h post-intraventricular injection of artificial CSF (aCSF), hemoglobin (HB), or HB + deferoxamine (HB+DFX) at post-natal day 4 (P4). AuNPs (brown/black) are observed in the ChP lumen and epithelium. A scale bars = 200 μm, B scale-bars = 25 μm. (C) Quantification of AuNP integrated density in the ChP shows a significant increase in AuNPs in the ChP 72 h after HB injection, which was reduced with DFX treatment at the time of IVH induction (HB injection). Data are mean ± SEM, n = 4 per group; one-way ANOVA with post-hoc Tukey test

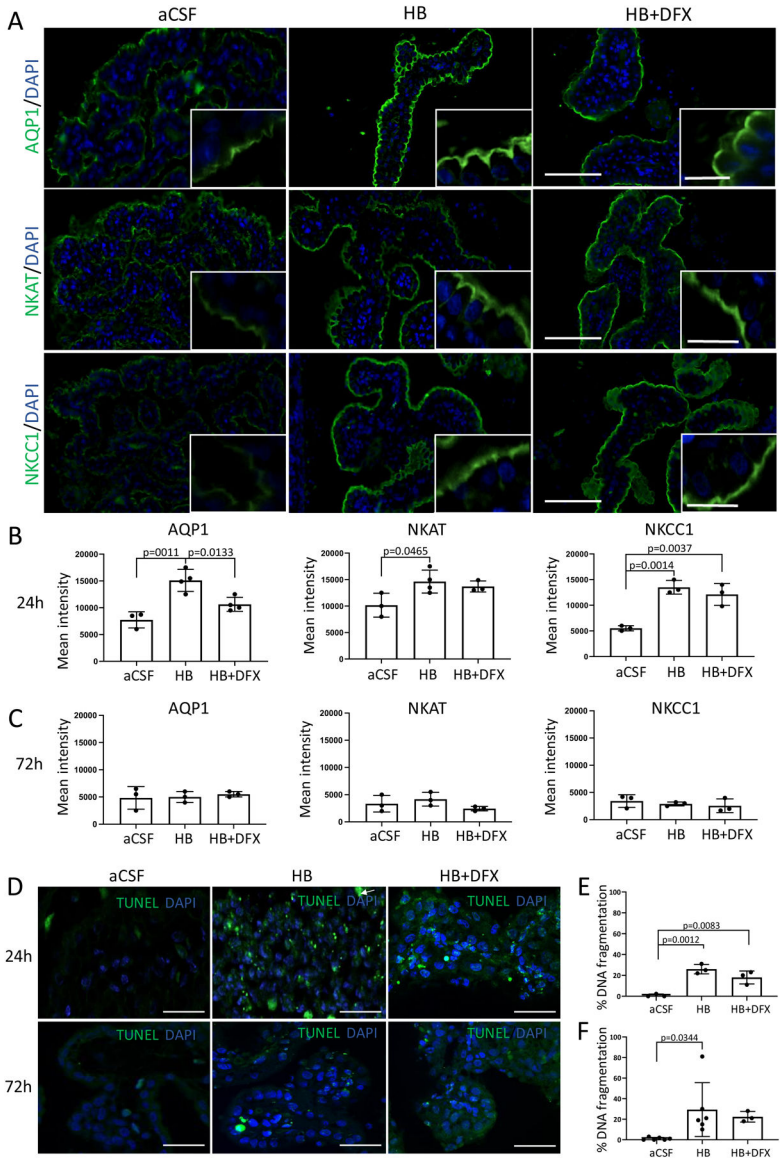

Figure 7. Hemoglobin (HB)-induced choroid plexus (ChP) expression of ion and water transporters.

(A) Representative immunofluorescence of lateral ventricle ChP aquaporin-1 (AQP1), Na+/K+/ATPase (NKAT), and Na+/K+/Cl- cotransporter 1 (NKCC1) expression 24 h after intraventricular injection of artificial CSF (aCSF), hemoglobin (HB), or HB + deferoxamine (DFX) in post-natal day 4 (P4) rats. Scale bars = 50 μm, inset scale bars = 10 μm. (B–C) Quantification of mean intensity of AQP1, NKAT, and NKCC1 expression 24 h (B) and 72 h (C) post-aCSF, HB, or HB + DFX injection showing a significant increase in AQP1 expression 24 h after IVH induction (HB injection), which was prevented by DFX treatment. Significant increases in NKAT and NKCC1 expression after IVH were not altered by DFX treatment. At 72 h post-injection, there were no significant differences in ChP expression of AQP1, NKAT, or NKCC1. Data are mean ± SEM, n = 3–4 per group; one-way ANOVA with post-hoc Tukey. (D) Representative images of right lateral ventricle ChP terminal deoxynucleotidyl transferase deoxyuridine triphosphate nick end labeling (TUNEL) assay

for DNA fragmentation 24 h and 72 h after intraventricular injection. Scale bars = 50 μm. (E–F) Quantification of cellular DNA fragmentation at 24 h (E) and 72 h (F) post-aCSF, HB, or HB + DFX injection. Data are mean ± SEM, n = 3–6 per group; one-way ANOVA with post-hoc Tukey test

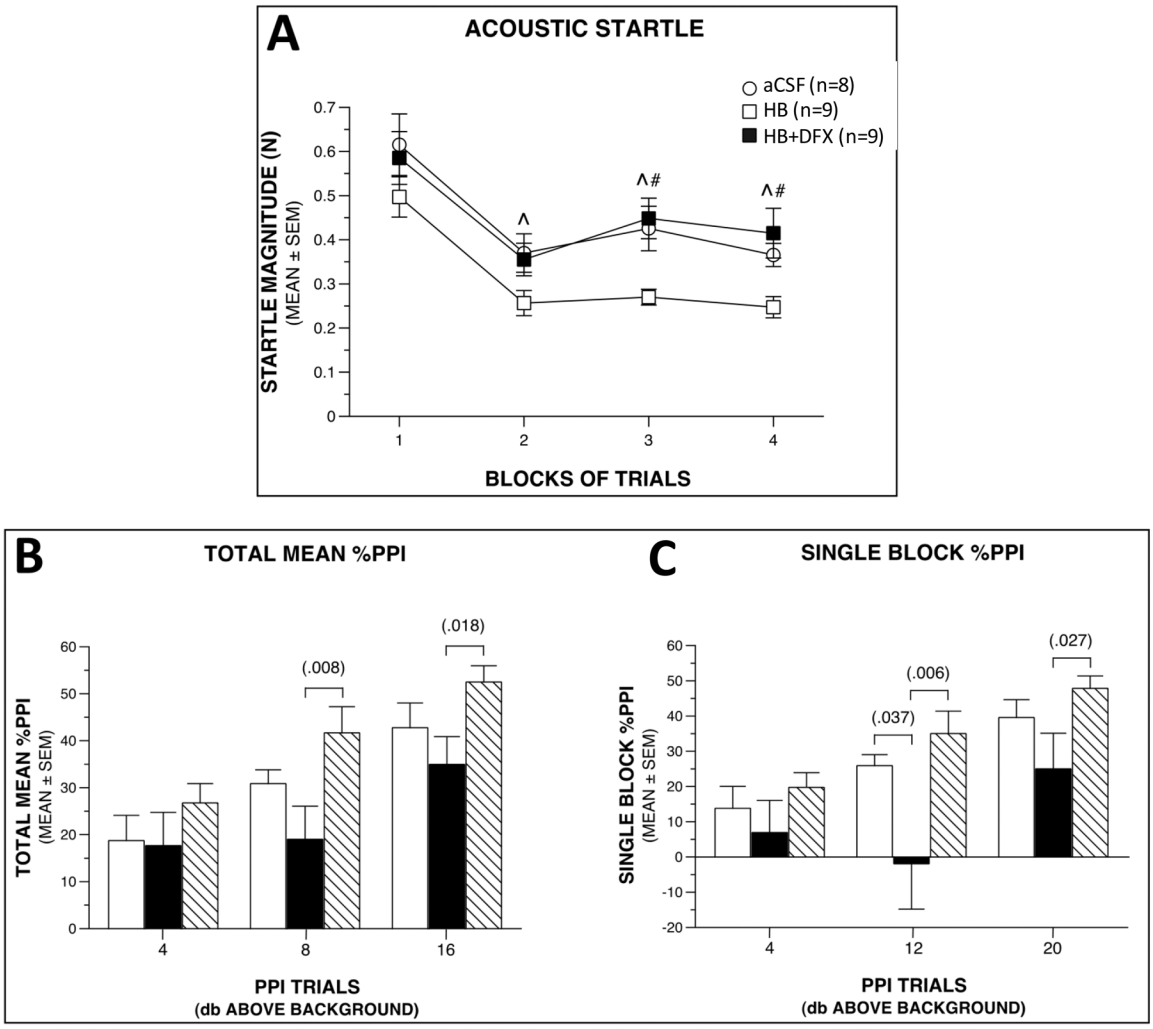

Figure 8. Deferoxamine (DFX) treatment restores acoustic startle response magnitudes to control-like levels following intraventricular hemorrhage and increases prepulse inhibition (PPI) response magnitudes.

(**A**) Deferoxamine (DFX) treatment restores acoustic startle response magnitudes to control-like levels following intraventricular hemorrhage and increases prepulse inhibition (PPI) response magnitudes. (A) Analysis of acoustic startle data after intraventricular injection of artificial CSF (aCSF control), hemoglobin (HB), or HB + DFX at post-natal day 4 (P4) shows that groups differed significantly in their response levels (treatment effect: $p = 0.025$). Subsequent simple effects tests showed that the HB-treated rats had significantly lower acoustic startle levels on average across blocks ($p = 0.023$) compared to aCSF controls with pair-wise comparisons showing differences occurring at blocks 2 (^$p = 0.040$), 3 (^$p = 0.012$), and 4 (^$p = 0.047$). Similarly, the startle response of the HB-treated rats was also significantly lower on average relative to the HB + DFX group ($p = 0.015$), with differences being observed at blocks 3 (#$p = 0.004$) and 4 (#$p = 0.005$). (B) The groups also differed with regard to the magnitudes of their mean %PPI responses (treatment effect: $p = 0.035$). Differences were mostly due to the HB-treated rats showing significantly reduced %PPI levels compared to the HB + DFX group, on average across the PPI trial types (p

= 0.011), with differences being found for 8 dB (#p = 0.008) and 16 dB (#p = 0.018) above background trials. (C) Similar results were found when a different method was used to calculate %PPI. Namely, the groups were found to differ significantly (treatment effect: p = 0.033), which was mostly due to the HB-treated rats showing significantly reduced %PPI values relative to the HB + DFX group (p = 0.033), on average across PPI trial types. Pair-wise comparisons showed that the differences between these two groups were greatest for the 12 dB (p = 0.006) and 20 dB (p = 0.027) above background trials. The simple effects test comparing HB vs. CSF was not significant (p = 0.081), although large differences were found during the 12 dB above background trial (p = 0.037). B-C white bars indicate aCSF, black bars indicate HB, striped bars indicate HB+DFX.